SSRG International Journal of Electronics and Communication Engineering
ISSN: 2348-8549/ https://doi.org/10.14445/23488549/IJECE-V13I6P109

Volume 13 Issue 6, 112-123, June 2026

Original Article

High-Power-Density Matrix-Converter UPQC for Bidirectional Power Quality Conditioning in Renewable-Integrated Microgrids

Naveen G[1*], Sangamesh G Sakri[1]

[1]*Department of Electrical and Electronics Engineering*
Poojya Doddappa Appa College of Engineering, Visvesvaraya Technological University, Kalaburagi, Karnataka, India.

[*]*Corresponding Author : gubba.naveen@ieee.org,*

Received: 11 March 2026 Revised: 09 April 2026 Accepted: 08 May 2026 Published: 27 June 2026

Abstract *- Power quality degradation in renewable-integrated microgrids remains a persistent concern as photovoltaic generation variability and nonlinear loading conditions introduce simultaneous harmonic distortion, voltage sag, swell, and unbalance that conventional compensation arrangements struggle to address within a single unified framework. Existing solutions based on the Voltage Source Inverter Unified Power Quality Conditioner (VSI-UPQC) and Active Power Filter (APF) topologies rely on electrolytic Direct Current (DC) link capacitor banks that introduce reliability limitations, increase passive component volume, and reduce full-load conversion efficiency under bidirectional battery operation. This paper presents a capacitorless Matrix Converter-Based Unified Power Quality Conditioner (MC-UPQC) employing Direct Quadrature (dq) frame control with Phase-Locked Loop (PLL) synchronisation and adaptive gain tuning to provide simultaneous series and shunt compensation in a three-phase four-wire (3ϕ-4W) microgrid. Measured solar irradiance data drawn from the National Renewable Energy Laboratory National Solar Radiation Database (NREL NSRDB), comprising Global Horizontal Irradiance (GHI), Direct Normal Irradiance (DNI), diffuse horizontal irradiance (DHI), and ambient temperature sampled over an eight-day window, was used to drive a 50 kW Photovoltaic (PV) generation profile across six disturbance scenarios evaluated in a MATLAB/Simulink R2023b environment using the Simscape Electrical toolbox. Simulation results show that the proposed MC-UPQC reduced source current Total Harmonic Distortion (THD) from 18.4% to 2.1%, lowered voltage unbalance factor (VUF) from 3.0% to 0.5%, restored Point of Common Coupling (PCC) voltage within 12 ms with a regulation error of 0.01 pu, and achieved 97.1% full-load efficiency with a power density of 2.4 kW/L, outperforming APF-only and conventional VSI-UPQC baselines.*

Keywords *- Matrix Converter, Unified Power Quality Conditioner, Microgrid Power Quality, Harmonic Mitigation, Voltage Sag Compensation, Bidirectional Power Flow, Adaptive Control*.

1. Introduction

The increasing penetration of distributed renewable energy sources in low-voltage distribution networks has changed the operating behaviour of modern microgrids. Solar Photovoltaic (PV) generation fluctuates with solar radiation, battery storage units bidirectionally exchange power with the grid, and nonlinear loads draw distorted currents from the local grid. When these components are connected at the same Point of Common Coupling (PCC), the power quality problem becomes a complex issue, rather than a simple harmonic or voltage regulation problem. It combines generation variability, voltage variation, current distortion, and load sensitivity. This makes local power quality management more difficult, especially in compact renewable microgrid installations [1]. PV systems create output profiles that vary with irradiance conditions, and when they share a PCC with nonlinear and sensitive loads, the interaction between them produces compound disturbances that passive mitigation measures cannot adequately suppress. Hence, active compensation topologies capable of handling multiple power quality impairments within a unified structure are required [2].

Voltage sag, voltage swell, harmonic distortion, and three-phase unbalance are among the most critical disturbances affecting renewable-integrated microgrids [3]. Harmonic currents injected by rectifier-based loads increase Total Harmonic Distortion (THD) at the PCC beyond the IEEE-519 limit. Voltage sag and swell events disturb sensitive load terminals within a few cycles, while unbalanced supply conditions increase stress on rotating machines and connected equipment over time [4]. While these issues often coexist in practical microgrids, many existing compensation techniques

address them in isolation. This creates a clear research gap. A unified compensation method that can simultaneously compensate harmonics, sag, and swell, unbalance, and is applicable for renewable energy systems with bidirectional battery operation, is not yet fully explored in the literature, especially with practical installation issues such as reliability, passive component volume, and converter efficiency taken into account [5].

Conventional compensation strategies address only part of this problem. Passive filters attenuate selected harmonic frequencies, but they cannot adapt to changing load patterns [6]. Active power filters (APFs) provide adaptive shunt compensation, but they do not correct series voltage disturbances such as sag and swell [7]. The Unified Power Quality Conditioner (UPQC), formed by series and shunt Voltage-Source Inverter (VSI) stages linked through a common Direct-Current (DC) capacitor bank, is closer to a complete compensation solution. Even so, the DC-link capacitor remains a major limitation. Banks of electrolytic capacitors decrease reliability under thermal cycling, increase the volume of passive components, and limit power density for space-constrained microgrid applications [8]. The intermediate DC stage may also impact bidirectional battery operation since extra conversion stages can cause losses and instability.

This paper reports on a capacitorless Matrix Converter-Based Unified Power Quality Conditioner (MC-UPQC), which eliminates the DC link capacitor stage by using direct Alternating Current (AC) to AC power conversion, thereby eliminating the main reliability limitation of the conventional designs, while simultaneously reducing the passive component volume and improving the conversion efficiency [9]. The proposed topology is operated in a three-phase four-wire (3ϕ-4W) microgrid with a Photovoltaic (PV) source and a bidirectional battery with a direct quadrature (dq) frame control scheme, Phase-Locked Loop (PLL) synchronization, and an adaptive gain tuning mechanism for simultaneous series and shunt compensation [10].

Solar irradiance data from the National Renewable Energy Laboratory (NREL) National Solar Radiation Database (NSRDB), which includes Global Horizontal Irradiance (GHI), Direct Normal Irradiance (DNI), Diffuse Horizontal Irradiance (DHI), and ambient temperature, were used to build a realistic PV generation profile over multiple disturbance scenarios. While existing APF and VSI-UPQC methods either offer limited compensation or rely on a DC-link capacitor stage, the proposed MC-UPQC provides a capacitorless direct AC-AC compensation system. This is the key contribution of the paper. It allows simultaneous harmonic compensation, sag/swell control, unbalance compensation, and bidirectional power-flow support in a single control structure. As such, the comparison with the prior research shows not only improvements in compensation performance, but also in compactness, efficiency, and reliability of the converter.

The main contributions of this work are summarized as follows:

- A capacitorless MC-UPQC topology for simultaneous series and shunt power quality compensation of a 3-phase-4-wire (3ph-4W) renewable microgrid is proposed by replacing the conventional Voltage Source Inverter (VSI) based DC link with direct AC-AC matrix conversion.
- An adaptive dq-frame control scheme with PLL synchronization and online gain adjustment is developed to achieve source-current Total Harmonic Distortion (THD) suppression according to the requirements of the IEEE 519.
- Voltage sag and swell regulation at the sensitive load terminal is demonstrated with faster settling time and lower regulation error as compared to a conventional VSI-UPQC under the same disturbance conditions.
- Bidirectional battery operation is featured in charge and discharge transitions, improvement in Point-Of-Common-Coupling (PCC) voltage deviation, transition time, full-load efficiency, and power density compared to the conventional VSI-UPQC reference.
- Public solar resource data from the NREL NSRDB are incorporated into the simulation workflow as a validated PV variability input, which provides a reproducible disturbance basis for the experimental evaluation.

The rest of this manuscript is structured as follows. Section II gives a review of the background related to UPQC topologies and matrix converter-based compensation. Section III describes the proposed MC-UPQC circuit topology and its adaptive control architecture. Section IV describes the simulation environment and the processing of the dataset, and the various disturbance scenarios considered. Section V discusses the simulation results. Section VI provides the concluding remarks, identifies the limitations, and proposes directions for future research.

2. Related Work

Numerous studies have addressed power quality improvement in renewable-integrated microgrids because photovoltaic generation, nonlinear loads, and storage interfaces often give rise to simultaneous voltage and current distortions. The conventional compensation mainly focused on passive filters and Active Power Filters (APFs). Passive filters are easy and cheap to implement, but they can only compensate for certain harmonic frequencies and cannot be adapted to varying loads. APFs offer improved compensation of harmonics and reactive power, particularly for nonlinear loads, but they primarily operate in the shunt path and cannot completely control the sag, swell, and unbalance of sensitive loads. As a result, Unified Power Quality Conditioner (UPQC)

systems, which combine series and shunt compensation, have gained popularity.

Recent research has enhanced UPQC control for renewable microgrids. Lukka et al. [11] applied an Adaptive Neuro-Fuzzy Inference System (ANFIS) to control a UPQC for compensation of power quality disturbances in renewable microgrids. This approach enhanced dynamic compensation, but it requires fine-tuning of membership functions and adequate training for various conditions. Abdulwahab et al. [12] used the Artificial Rabbit Search optimisation algorithm to optimise UPQC parameters for microgrids with nonlinear loads. The optimisation method enhances parameter tuning, but its computational complexity and simulation-based testing prevent its direct application in real-time systems. Espinosa Gutiérrez and Aguila Téllez [13] explored optimal placement of UPQC in distribution networks through exhaustive search. This approach optimises the selection of voltage profiles in small networks, but the search process is less feasible for larger networks, and the cost of UPQC installation was not considered.

Machine learning and intelligent controllers have also been proposed to enhance UPQC response to dynamic conditions. Kanchana et al. [14] used a Gated Recurrent Unit (GRU) controller in a PV-UPQC system to control distortion under dynamic operating conditions. The learning controller enhances flexibility, but its generalisation is unknown. Abbasi et al. [15] developed a power quality optimisation approach for a three-phase microgrid with a grid-connected photovoltaic source and battery storage, considering nonlinear loads and focusing on IEEE-519 standards. The framework is valuable for coordinated control, but its effectiveness is highly dependent on modelling assumptions and load characteristics. Rajesh et al. [16] proposed a hybrid control approach for managing photovoltaic, wind, fuel-cell, and battery power sources to enhance microgrid power quality. While the multi-source approach enhances flexibility, it also complicates tuning and generalisation to different microgrid configurations.

Other research has considered inverter operation, islanding, and renewable energy. Dagar et al. [17] studied the impact of islanding detection using q-axis current injection on source current Total Harmonic Distortion (THD) and Total Demand Distortion (TDD). The results are helpful to understand the distortion caused by inverters, but their design guidelines are constrained to simulation settings and do not account for hardware variation. Subramaniam and Sundararaju [18] developed an enhanced UPQC integration scheme for solar PV systems to improve power quality. The approach exhibits better compensation in the proposed system, but it is dependent on system assumptions. Samala and Bethi [19] surveyed hybrid renewable energy systems and their impact on UPQC-based power quality. This review is informative, but it does not present a practical compensation topology or control scheme. Ajewole et al. [20] applied reinforcement learning brainstorm optimisation to optimise UPQC operation in hybrid-source microgrids for standards-compliant power quality. The approach is promising, but the stability of training, safety constraint satisfaction, and generalisation over different grid topologies need to be further validated.

As reviewed, it can be noted that the most recent research efforts are on controller optimisation, intelligent tuning, DER coordination, or placement strategy. This work enhances certain aspects of UPQC operation, but many of them still adopt the traditional Voltage-Source Inverter (VSI)-based UPQC with a Direct-Current (DC) link capacitor. This capacitor stage increases passive component count, decreases power density, and poses a reliability problem under thermal and bidirectional power-flow conditions. Another concern is that many studies test their techniques under limited or constant disturbance conditions, which do not reflect the practical operation of a renewable microgrid where harmonic distortion, voltage sag/swell, unbalance, PV variability, and battery power reversal may coexist.

This work overcomes these limitations by developing a capacitorless matrix converter-based UPQC for a three-phase four-wire renewable microgrid. The proposed topology is based on direct AC-AC conversion, eliminating the need for the DC-link capacitor. The control scheme integrates dq-frame compensation, Phase-Locked Loop (PLL) synchronisation, and adaptive gain control to achieve simultaneous series and shunt compensation. The system is tested under six disturbance scenarios, with solar input from the National Renewable Energy Laboratory (NREL) National Solar Radiation Database (NSRDB). Therefore, the study advances work both in terms of the topology, by eliminating bulky passive components, and in terms of the evaluation of the compensation scheme, by considering a wider operating envelope of the renewable microgrid.

3. Materials and Methods

3.1. Overall Microgrid Architecture

The test system is set up as a three-phase four-wire (3ϕ-4W) low-voltage microgrid which operates at a Point Of Common Coupling (PCC) with a line-to-line voltage of 415 V at 50 Hz. It consists of a 50 kW PV array, a 30 kW Bidirectional Battery Energy Storage System (BESS), and a mixed load configuration of a 20 kVA nonlinear load, a 15 kVA Resistive-Inductive (RL) load, and a 10 kVA sensitive load, connected via a common AC bus as shown in Figure 1. A 30kVA MC-UPQC is proposed to be inserted at the PCC in order to provide simultaneous series and shunt compensation and eliminate the intermediate DC link stage characteristic of conventional voltage-source inverter (VSI)-based topologies. The series MC-UPQC stage is connected in series with the supply path through a series transformer, while the shunt MC-UPQC stage is connected to the PCC bus through an LC filter,

which consists of L=2.5 mH and C=10 uF per phase, as shown in Figure 1. Irradiance and temperature inputs from the National Renewable Energy Laboratory's National Solar Radiation Database (NREL NSRDB), which include GHI, DNI, DHI, and ambient temperature, are used to produce the PV array production profile. The BESS has bidirectional interfaces at ±20 kW to manage the power balance between generation and load demand. The instantaneous three-phase supply voltage is used as the compensation reference throughout the study.

$$v_{s,abc}(t) = V_s \sin(\omega t + \phi_{abc}) \quad (1)$$

where V_s is the peak phase voltage, ω is the fundamental angular frequency, and ϕ_{abc} denotes the respective phase angles. The expression in (1) defines the ideal undistorted reference against which all compensation targets are evaluated.

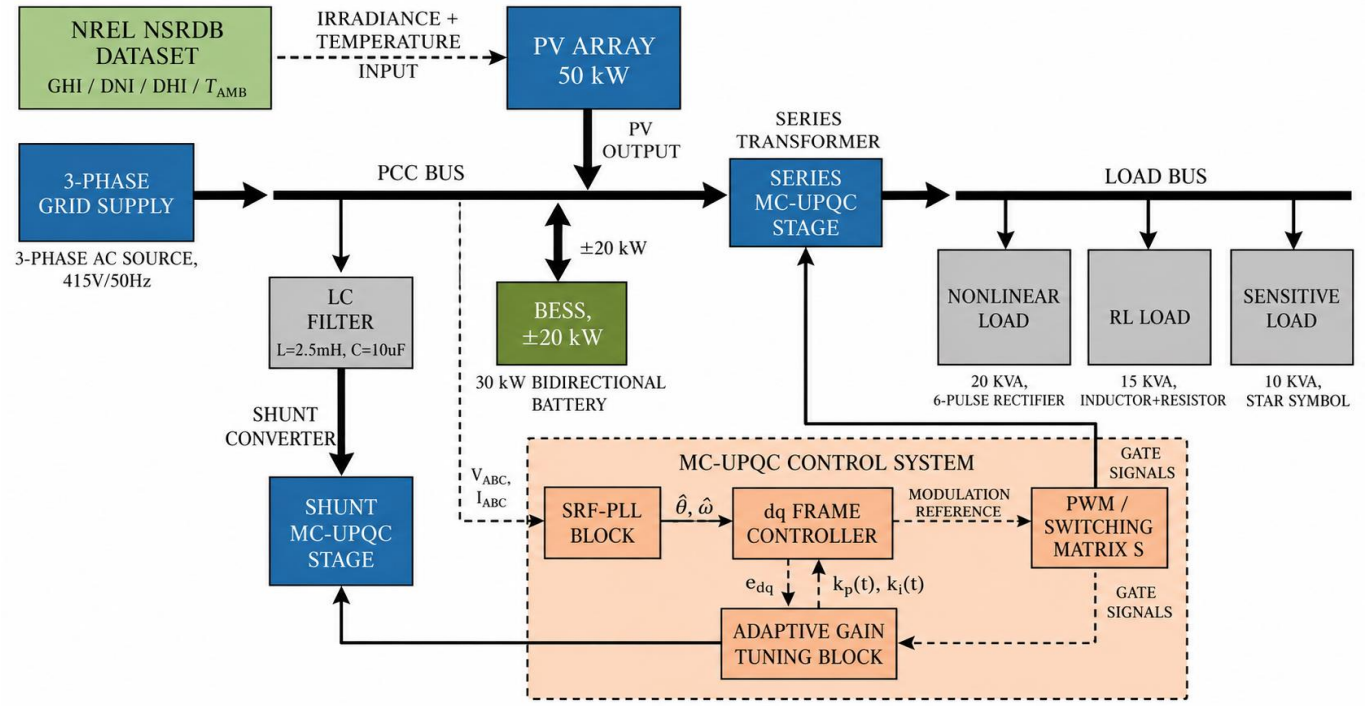

Fig. 1 System architecture of the proposed MC-UPQC in a 3ϕ-4W microgrid

3.2. Matrix Converter Topology and Switching Constraint

The Matrix Converter (MC) realises direct AC-AC power conversion through a 3×3 bidirectional switch array that connects each input phase to any output phase without requiring an intermediate energy storage element. The output voltage vector is related to the input through the switching matrix S as

$$v_{out} = S \cdot v_{in} \quad (2)$$

and the corresponding input current vector follows from the transpose relationship $i_{in} = S^T \cdot i_{eut}$. The relationship in (2) confirms that the matrix converter maintains instantaneous power balance between input and output ports without capacitive energy buffering, which is the physical basis for the compactness and efficiency improvements over conventional VSI-UPQC designs. Each bidirectional switching cell is based on back-to-back Insulated-Gate Bipolar Transistors (IGBTs); the switching frequency is maintained to 10 kHz, and the LC output filter consists of an inductance of 2.5 mH and a capacitance of 10 μF/phase, which is used to suppress high-frequency switching harmonics before the injection of the compensation voltage.

3.3. Phase-Locked Loop Synchronisation

The systems require precise phase detection to enable their series and shunt compensation operations, which the system achieves through its synchronous reference frame phase-locked loop SRF-PLL that provides real-time supply phase angle. $\hat{\theta}$ measurements. The three-phase supply voltages are projected onto the synchronous dq frame through the combined Clarke and Park transformation, which produces d-axis and q-axis voltage components. v_d and v_q respectively. The system locks properly when the q-axis component reaches zero because the error signal gets processed through a proportional-integral PI regulator, which updates the estimated angular frequency.

$$\hat{\omega}(t) = \omega_0 + k_p \cdot v_q(t) + k_i \int_0^t v_q(\tau)\, d\tau \quad (3)$$

where ω_0 is the nominal angular frequency, and k_p, k_i are the PLL regulator gains. The tracked phase angle $\hat{\omega}$ is then obtained by integrating ω̂ and serves as the common synchronisation reference for both the series injection and shunt compensation controllers throughout all disturbance scenarios.

3.4. Series Compensation for Voltage Sag, Swell, and Unbalance

The series compensation path injects a controlled voltage in series with the supply line through a series transformer to restore the sensitive load terminal voltage during sag, swell, and unbalance events. The necessary injection voltage calculation uses the measured supply voltage together with the nominal dq-frame reference and the resulting regulation error to determine the value.

$$e_{dq}(t) = v_{Ref,dq}(t) - v_{L,dq}(t) \quad (4)$$

where $v_{Ref,dq}$ is the nominal voltage reference and $v_{L,dq}$ is the actual load terminal voltage in the dq frame, which is processed through a PI controller to generate the series modulation reference. Voltage unbalance is treated by separating the supply into positive and negative sequence components using the symmetrical component transform, and the Voltage Unbalance Factor (VUF) is measured as

$$VUF = \left(\frac{|V_-|}{|V_+|}\right) \times 100\% \quad (5)$$

where $|V_-|$ and $|V_+|$ are the negative and positive sequence voltage magnitudes, respectively. The system uses a single injection path, which allows it to correct both magnitude deviation and phase asymmetry through the combination of series injection reference and negative sequence compensation term that results from this decomposition method.

3.5. Shunt Compensation for Harmonic and Reactive Current Suppression

The shunt compensation path locally supplies the harmonic and reactive current demand of the nonlinear load at the PCC and prevents these current components from propagating into the supply network.

The instantaneous real and imaginary power quantities are calculated in the stationary $\alpha\beta$ frame according to the instantaneous power theory as

$$p = v_\alpha i_\alpha + v_\beta i_\beta , \quad q = v_\beta i_\alpha - v_\alpha i_\beta \quad (6)$$

where $v_{\alpha\beta}$ and $i_{\alpha\beta}$ are the supply voltage and load current components in the stationary frame. The power quantities in (6) show two components, which include a direct current component that results from fundamental frequency exchange and an oscillating component that stems from harmonic content. The shunt compensation reference is created by the selection of the oscillating active power, full reactive power, and harmonic current components for local supply, such that only the fundamental active component is drawn from the upstream network, and effectively both power factor and harmonic distortion are corrected with the same shunt injection stage.

3.6. Adaptive Gain Tuning

The fixed-gain controller structure fails to handle multiple disturbance scenarios because it needs different gain settings for sag compensation, harmonic suppression, and bidirectional power reversal operations. To handle this, an adaptive gain tuning layer continuously adjusts the series PI controller gains based on the instantaneous regulation error magnitude defined in (4), following the update law.

$$k_p(t) = k_{p,0} + \mu_p \, |e_{dq}(t)| \quad (7)$$

where $k_{p,0}$ is the nominal baseline gain and μ_p is a positive adaptation rate constant. The integral gain follows an analogous expression integrating the error magnitude over time. The mechanism in (7) increases the controller bandwidth proportionally to the observed deviation during large transient events such as sag onset and swell inception, and relaxes toward nominal values as the error diminishes in steady state, removing the need to schedule separate gain tables across operating modes and allowing a single controller structure to handle the full scenario set without manual retuning.

3.7. PV Power Mapping from NREL NSRDB Data

The PV generation profile is derived from irradiance and temperature records obtained from the NREL NSRDB and mapped to array output power through the scaling expression.

$$P_{PV}(t) = P_{rated} \cdot \left[\frac{G(t)}{G_{STC}}\right] \cdot [1 + \gamma_T (T_{cell}(t) - T_{STC})] \quad (8)$$

where P_{rated} is the rated output at Standard Test Conditions (STC), $G(t)$ is the instantaneous irradiance derived from the GHI, DNI, and DHI components, $G_{STC} = 1000\ \mathrm{W/m^2}$ is the STC irradiance reference, γ_T is the temperature coefficient of power, and $T_{STC} = 25°C$.

The cell temperature $T_{cell}(t)$ appearing in (8) is estimated from the ambient temperature record and the Nominal Operating Cell Temperature (NOCT) specification. The power sequence generated by (8) produces the time-varying PV injection profile, which drives the ramp variability and generation fluctuation scenarios that use missing irradiance samples, which were addressed through linear interpolation before applying the mapping expression.

4. Results and Discussion

This section describes the experimental findings of the ANN-based spectrum sensing model and compares the results with conventional techniques.

Table 1. Dataset and usage

Item	Value
Dataset	NREL NSRDB (National Solar Radiation Database)
Data Type	Solar resource time-series
Used For	PV power variability profile for microgrid PQ testing
Variables Used	GHI, DNI, DHI, Ambient Temperature
Sampling Interval	30 minutes
Duration Used	7 days + 1 high-variability day
PV Mapping Method	Irradiance/temperature → PV output scaling (50 kW PV)
Missing Data Handling	Linear interpolation
Output Generated	PV ramp events + fast variability windows

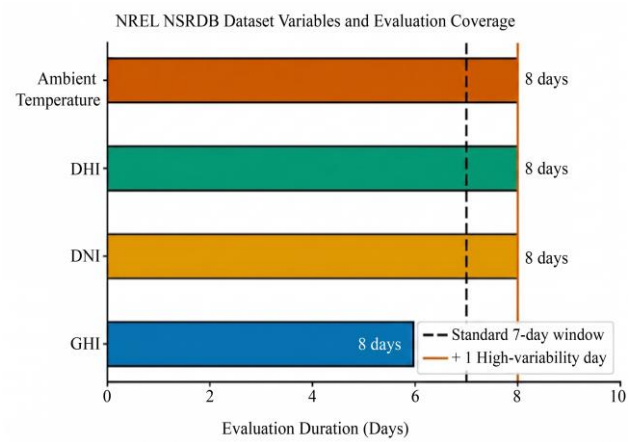

Fig. 2 NREL NSRDB dataset variables (GHI, DNI, DHI, ambient temperature) and eight-day evaluation coverage, with the standard seven-day window and additional high-variability day marked

Table 2. Microgrid and Converter test configuration

Parameter	Value
Grid / Microgrid Type	3ϕ AC microgrid (3ϕ–4 wire)
PCC Voltage / Frequency	415 V (L-L), 50 Hz
PV Rating	50 kW
Battery Rating	30 kW (bidirectional)
Loads	20 kVA nonlinear + 15 kVA RL + 10 kVA sensitive load
UPQC Rating	30 kVA
Proposed Topology	Matrix-converter-based UPQC (capacitorless)
Switching Frequency	10 kHz
Filter (per phase)	L = 2.5 mH, C = 10 μF
Control	dq control + PLL + adaptive gain tuning
Baselines	No Comp, APF-only, Conventional VSI-UPQC

4.1. Dataset Selection and Solar Resource Mapping

The simulation framework is based on measured data of solar irradiance from the NREL National Solar Radiation Database (NSRDB), which provides high temporal resolution records that can be used to capture realistic PV generation variability. As summarized in Table 1 and shown in Figure 2, three irradiance components were extracted, i.e., GHI, DNI, and DHI, in addition to the ambient temperature readings, all sampled at 30 min intervals.

A continuous seven-day window was chosen for standard operating conditions, with one day of extra high variability to stress test the compensation scheme under rapid fluctuations of generation. Where there were occasional gaps in the data, linear interpolation was used before processing. The measured irradiance and temperature values were then scaled to reflect the behavior of a 50 kW rooftop PV array to generate realistic ramp sequences and short-duration variability windows that are used as power quality disturbance inputs to the microgrid test environment.

4.2. Microgrid Architecture and Converter Setup

Irradiance and temperature data from the NREL NSRDB are included via interpolated look-up tables and are directly connected to the PV array block. Each of the disturbance scenarios is carried out as a separate Simulink configuration using the ode45 solver with a tolerance of 10^{-6} to ensure consistency of the results. The test platform is based on a three-phase four-wire ac microgrid with a Point of Common Coupling (PCC) voltage of 415 V line-to-line and nominal frequency of 50 Hz, as presented in Table 2.

The generation and storage assets include a 50 kW PV generation source and a 30 kW bidirectional battery unit, which feed into a mixed load profile comprising a 20 kVA nonlinear load, a 15 kVA resistive-inductive load, and a 10 kVA sensitive load segment. A 30 kVA matrix converter-based UPQC topology, designed without bulky DC link capacitors, is located at the PCC to handle simultaneous series and shunt compensation. The converter switching frequency is fixed at 10 kHz, and the filtering for each phase is done with a 2.5 mH inductor and a 10 μF capacitor.

Closed-loop regulation is implemented by means of a dq-frame current and voltage controller with a phase-locked loop and an adaptive gain adjustment mechanism. Three reference configurations, an uncompensated baseline, an active power filter only arrangement, and a conventional VSI-based UPQC, are included alongside the proposed topology in order to allow

a structured performance comparison among all the evaluated scenarios. The microgrid model was completely implemented in MATLAB/Simulink R2023b using the Simscape Electrical toolbox. Within this environment, the matrix converter, dq-frame controller, PLL, and adaptive gain tuning blocks were set to work with a fixed simulation time step of $1\mu s$ to maintain the numerical stability at the 10 kHz switching frequency.

Irradiance and temperature data from the NREL NSRDB were imported in the form of interpolated lookup tables and directly coupled to the PV array block. Each of the disturbance scenarios was run as a separate Simulink configuration using the ode45 solver with a tolerance of 10^{-6} to ensure consistency of the results.

4.3. Disturbance and Operating Scenario Definitions

The study assessed the proposed matrix-converter-based UPQC through six operating scenarios, which simulated common disturbances that microgrids experience according to Table 3 and Figure 3. Voltage sag and swell events were introduced at 0.7 pu and 1.2 pu, respectively, each persisting for 200 ms, which is representative of typical short-duration supply variations arising from upstream switching or fault clearance activities.

A continuously operating 6-pulse rectifier was used to generate nonlinear load harmonics throughout the entire simulation period under scenario S3, while a sustained voltage unbalance of 3% VUF was imposed for 1 s under scenario S4 to examine the asymmetrical compensation response.

Scenarios S5 and S6 were introduced to capture the dynamic character of renewable-integrated microgrids, where a PV generation ramp spanning 20% to 90% output was applied over a 60 s window, followed by a bidirectional battery power transition of ±20 kW maintained over 30 s. Together, these scenarios cover a sufficiently wide operating envelope to draw meaningful conclusions about both steady-state and transient compensation performance.

Table 3. Disturbance and Operating scenarios

Scenario	Condition	Magnitude	Duration
S1	Voltage Sag	0.7 pu	200 ms
S2	Voltage Swell	1.2 pu	200 ms
S3	Nonlinear Load Harmonics	6-pulse rectifier ON	Continuous
S4	Voltage Unbalance	3% VUF	1 s
S5	PV Variability Ramp	20% → 90% PV	60 s
S6	Bidirectional Power Flow	Battery ±20 kW	30 s

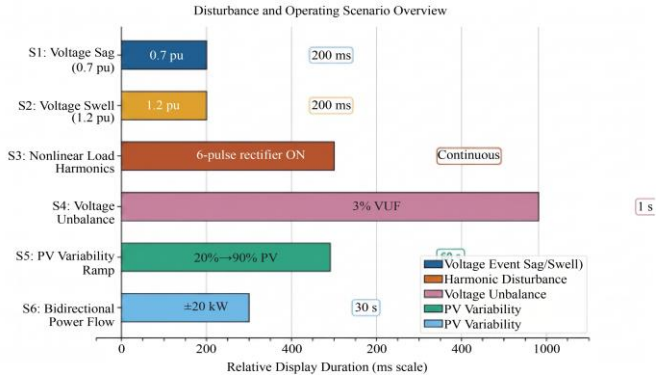

Fig. 3 Six simulation disturbance scenarios (S1–S6) covering voltage sag, swell, nonlinear harmonics, voltage unbalance, PV variability ramp, and bidirectional battery power flow with respective magnitudes and durations

4.4. Harmonic Mitigation Performance at the Point of Common Coupling

Harmonic distortion in the source current was measured before and after electronic compensation for each of the evaluated circuit topologies. The pre-compensation Total Harmonic Distortion (THD) was recorded uniformly at 18.4%, thus providing a consistent and repeatable disturbance baseline as detailed in Table 4 and illustrated in Figure 4. In the uncompensated configuration, the full distortion was maintained, thus not meeting the 5% criterion of the IEEE-519. The insertion of an active power filter only reduced the THD to 4.9 per cent, which resulted in a reduction of 73.4 per cent and slightly satisfied the stipulation. Subsequent incorporation of the conventional voltage-source inverter unregulated power quality conditioner (VSI-UPQC) further mitigated the THD to 3.2%, corresponding to an 82.6% reduction. The proposed Multi-Chip UPQC (MC-UPQC) showed the highest suppression with a post-compensation THD of 2.1% and an overall attenuation of 88.6%; this value is easily in compliance with the standard requirement of the performance of the device at the level of the Standard 519, with a satisfactory margin. The observed progressive improvement in the four experimental configurations emphasizes the benefit of combining direct AC-AC conversion with an adaptive control architecture to eliminate the harmonic injection pathways inherent in intermediate DC-link stages in conventional designs.

Table 4. Harmonic mitigation at PCC (Source Current THD)

Method	THD Before (%)	THD After (%)	THD Reduction (%)	IEEE-519 (<5%)
No Compensation	18.4	18.4	0.0	×
APF Only	18.4	4.9	73.4	✓
Conventional VSI-UPQC	18.4	3.2	82.6	✓
Proposed MC-UPQC	18.4	2.1	88.6	✓

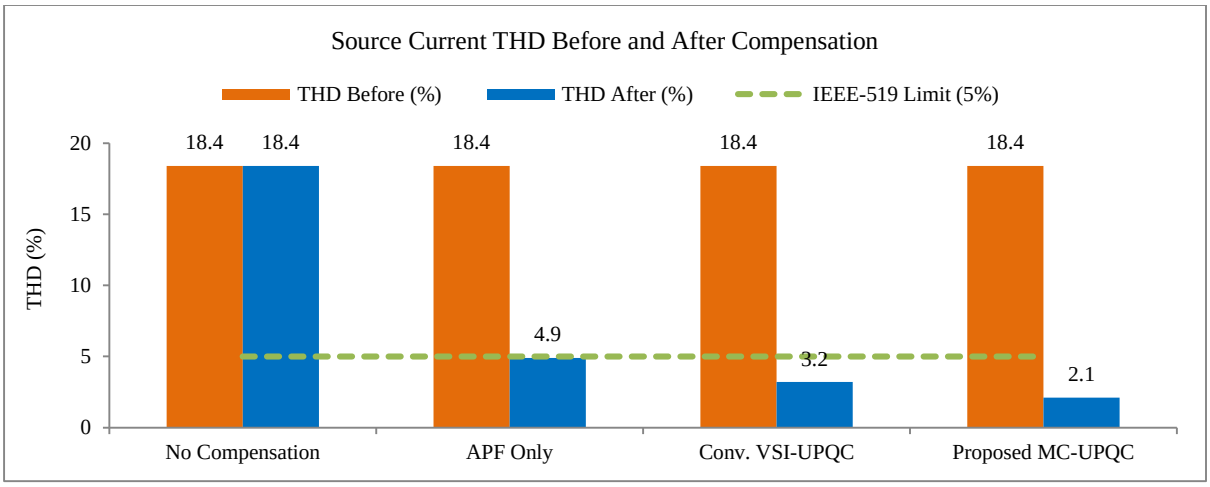

Fig. 4 Source current THD before and after compensation for all evaluated topologies against the IEEE-519 limit of 5%. The proposed MC-UPQC achieves the lowest post-compensation THD of 2.1%

4.5. Voltage Sag and Swell Compensation Performance at the Sensitive Load Terminal

The ability of the proposed topology to control the sensitive load voltage in the event of short-duration supply disturbances was evaluated under two scenario conditions, i.e., a 0.7 pu voltage sag and a 1.2 pu voltage swell, with the measured quantities of all three compensation configurations listed in Table 5 and Figure 5. Prior to any disturbance, each method had the same pre-event voltage of 1.00 pu, which set a common reference point from which the transient response of each configuration could be fairly compared. When the sag event was applied under scenario S1, the uncompensated case allowed the load voltage to collapse fully to 0.70 pu, settling at that depressed value with a regulation error of 0.30 pu, an overshoot of 9.0%, and a load voltage THD of 6.8%, confirming the complete absence of any corrective action across the 160 ms observation window. The conventional VSI-UPQC maintained a voltage dip at 0.97 pu and restored the steady-state voltage to 1.00 pu within 18 milliseconds while the regulation error decreased to 0.03 pu, the overshoot dropped to 3.5%, and the load THD reached 2.4%. The proposed MC-UPQC further restricted this response, keeping the minimum voltage during the sag at 0.99 pu, which restored steady state in only 12 ms, resulting in a regulation error of only 0.01 pu with an overshoot of 2.0% and a load THD of 1.6%, all of which are measurable and consistent improvements over the VSI-based counterpart. Turning to the swell condition for scenario S2, the uncompensated case again indicated the full undisturbed disturbance magnitude with the load voltage increasing to 1.20 pu and staying elevated with a regulation error of 0.20 pu, an overshoot of 7.5%, and a THD of 5.9% persisting over the 150 ms window. The VSI-UPQC limited the peak voltage to 1.03 pu and returned to nominal in 20 ms with a regulation error of 0.03 pu and an overshoot of 3.0%, and a load THD of 2.1%. The proposed MC-UPQC again outperformed this result by limiting the peak voltage to only 1.01 pu, settling the load in 13 ms, and producing a regulation error of 0.01 pu, an overshoot of 1.8%, and a load THD of 1.5%. Taken together, the results of the sag and swell tests show that the matrix-converter topology with the lack of a DC-link capacitor and the tighter bandwidth provided by the adaptive gain tuning layer always provides a faster voltage recovery, lower residual error, and reduced waveform distortion as compared to the conventional VSI-UPQC configuration in both over-voltage and under-voltage disturbance types.

Table 5. Compact Sag/Swell compensation (Sensitive Load)

Scenario	Method	Vpre (pu)	Vmin/max during event (pu)	Vsteady after (pu)	Settling (ms)	Reg. Error (pu)	Overshoot (%)	Vload THD (%)
S1: Sag (0.7 pu)	No Comp	1.00	0.70 (Vmin)	0.70	160	0.30	9.0	6.8
	VSI-UPQC	1.00	0.97 (Vmin)	1.00	18	0.03	3.5	2.4
	Proposed MC-UPQC	1.00	0.99 (Vmin)	1.00	12	0.01	2.0	1.6
S2: Swell (1.2 pu)	No Comp	1.00	1.20 (Vmax)	1.20	150	0.20	7.5	5.9
	VSI-UPQC	1.00	1.03 (Vmax)	1.00	20	0.03	3.0	2.1
	Proposed MC-UPQC	1.00	1.01 (Vmax)	1.00	13	0.01	1.8	1.5

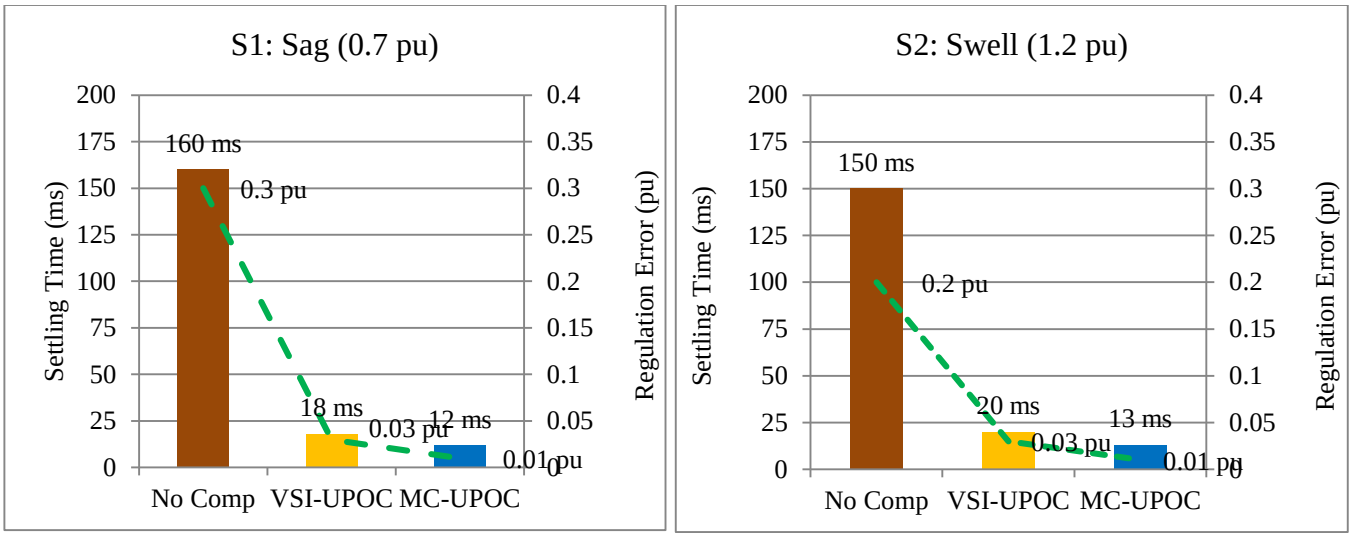

Fig. 5 Settling time and regulation error under voltage sag S1 (0.7 pu) and swell S2 (1.2 pu) for the uncompensated baseline, VSI-UPQC, and proposed MC-UPQC

4.6. Voltage Unbalance Suppression and Power Factor Correction Across Compensation Methods

The degree to which each of the compensation configurations effectively alleviated simultaneous voltage unbalance and reactive power deficiency is summarised in Table 6, where the four methodologies all began from a common pre-compensation voltage unbalance factor of 3.0% and power factor of 0.86, thereby providing an identical starting point to allow fair attribution of post-compensation improvements to each topology rather than to divergent starting operating points. The uncompensated baseline held both parameters constant, which agreed with neither the unbalance nor the lagging power factor being passively resolved under the imposed load conditions. The introduction of the APF-only configuration lowered the VUF to 2.1%, which is evidence of a partial but incomplete suppression of the phase asymmetry, while the power factor improved to 0.95, which is evidence that the shunt filtering provides meaningful reactive compensation even without a series voltage regulation path.

The conventional VSI-UPQC obtained a much lower VUF of 0.8% and improved the power factor to 0.99, which is the combination of the coordinated interaction of series and shunt converter stages operating in a unified control framework. The proposed MC-UPQC provided the best results in terms of both metrics, further improving the VUF to 0.5% and achieving a power factor of 0.995, which is practically unity and unlikely to be bettered by any passive or partially active corrective arrangement, as shown in Figure 6. The marginal but consistent superiority over the VSI-UPQC in both metrics suggests that the removal of the DC-link capacitor and subsequent reduction of the internal reactive circulation within the converter plays at least a small part in the tighter phase balancing and slightly superior reactive power tracking that is seen in steady state operation.

Table 6. Unbalance (VUF) and Power factor improvement

Method	VUF Before (%)	VUF After (%)	PF Before	PF After
No Compensation	3.0	3.0	0.86	0.860
APF Only	3.0	2.1	0.86	0.950
Conventional VSI-UPQC	3.0	0.8	0.86	0.990
Proposed MC-UPQC	3.0	0.5	0.86	0.995

4.7. Bidirectional Power Flow Behaviour, Converter Efficiency, and Physical Compactness

A comparative evaluation of the conventional VSI-UPQC and the proposed MC-UPQC under bidirectional battery operation, full-load efficiency conditions, and physical volume considerations is presented in Table 7, which covers eight individual performance metrics that collectively characterise the suitability of each topology for practical microgrid deployment. During the discharge of the battery, the source current THD measured at the PCC was 3.4% and 2.3% for the VSI-UPQC and proposed topology, respectively, whereas the charge mode THD values were 3.6% and 2.4%, respectively, showing that the MC-UPQC has a more consistent waveform quality regardless of the direction of power transfer through the storage interface. The PCC voltage deviation measured during the bidirectional power reversal at ±20 kW has been measured to ±0.030 pu for the VSI-UPQC, while the proposed converter limited the PCC voltage deviation to ±0.015 pu, which is especially significant for sensitive load segments, which are sensitive even to short-lasting excursions outside their rated voltage tolerance band. The power reversal transition time, which describes the speed at which the converter re-enters regulated operation after a change in battery current direction, was 30 ms for the VSI-

UPQC and shortened to 18 ms for the proposed MC-UPQC, a difference that can be explained by the lack of DC-link capacitor charge redistribution dynamics that can usually cause additional delay in polarity transitions in conventional two-stage topologies. At full load operation, the MC-UPQC achieved an efficiency of 97.1% compared to 95.6% for the VSI-UPQC, with total converter losses of 710 W and 920 W, respectively, which represents a loss of 210 W that accumulates significantly over long periods of operation and corresponds to lower thermal management requirements at the component level. The passive component volume of the proposed converter was found to be 0.72 times that of the VSI-UPQC reference and the corresponding power density went from 1.8 kW/L to 2.4 kW/L, which together validate the fact that the elimination of the electrolytic DC-link capacitor bank not only removes a known reliability limitation, but also results in a physically more compact assembly that is better suited to space constrained microgrid enclosures where converter footprint is a practical installation constraint rather than merely a secondary design consideration.

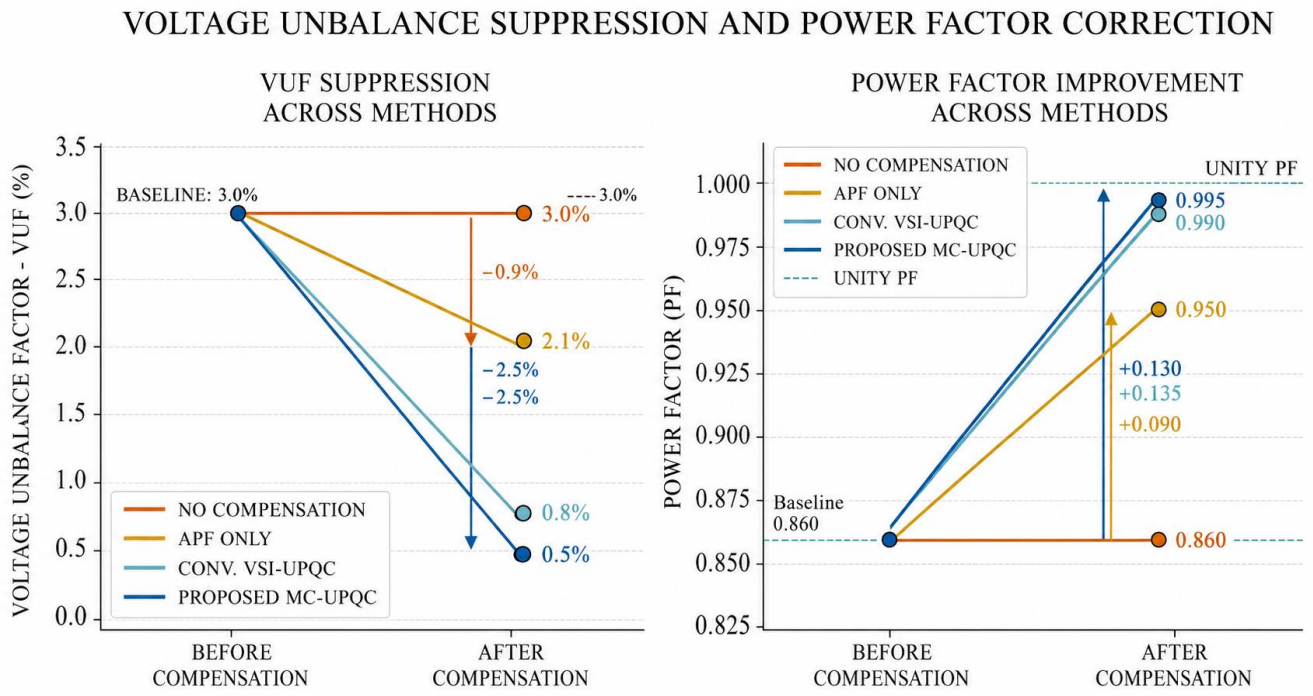

Fig. 6 VUF suppression and power factor improvement from the pre-compensation baseline to the post-compensation outcome for each evaluated method

Table 7. Bidirectional operation, efficiency, and Power density

Metric	Conv. VSI-UPQC	Proposed MC-UPQC
THD during Battery Discharge (%)	3.4	2.3
THD during Battery Charge (%)	3.6	2.4
PCC Voltage Deviation during ±20 kW (pu)	±0.030	±0.015
Power Reversal Transition Time (ms)	30	18
Full-load Efficiency (%)	95.6	97.1
Total Converter Loss at Full-load (W)	920	710
Passive Component Volume (relative)	1.00×	0.72×
Estimated Power Density (kW/L)	1.8	2.4

5. Discussion

The simulation results as a whole show that the matrix-converter-based UPQC provides measurable and consistent improvements in all the power quality aspects considered when compared with the uncompensated baseline, the APF-only arrangement, and the conventional VSI-UPQC. Harmonic distortion at the PCC was reduced from a pre-compensation level of 18.4% to 2.1% with an attenuation of 88.6%, well within the requirement of the IEEE-519 with a good margin. In comparison, the APF-only and VSI-UPQC configurations had attenuation values of 4.9 and 3.2 percent, respectively, both of which have comparatively less headroom compared to the 5 percent threshold. Voltage sag and swell control at the sensitive load terminal only reinforced this trend.

The proposed topology kept the sag minimum value at 0.99 pu and achieved steady state in 12 ms at a regulation error of only 0.01 pu, which is quite tight compared to the VSI-UPQC results of 0.97 pu and 18 ms under the same disturbance conditions. The swell response was similar, with the MC-UPQC capping the peak at 1.01 pu and settling in 13 ms, versus 1.03 pu and 20 ms for the VSI-UPQC. These observations suggest that the lack of a DC-link capacitor and the more dynamic response of the adaptive gain-tuning layer are a combined effect in the observed improvement in transient-tracking fidelity. Voltage unbalance suppression reduced the VUF from an initial value of 3.0% to 0.5% for the proposed topology, compared with 0.8% for the VSI-UPQC. Simultaneously, the power factor was 0.995, a value which is practically indistinguishable from unity and is substantially improved over the 0.99 measured by the conventional counterpart. Under bidirectional battery operation, the MC-UPQC kept the source-current THD below 2.4% in both charge and discharge mode, the PCC voltage deviation within ±0.015 pu during ±20 kW power reversals, and completed the transition from one of the flow directions to the other in 18 ms compared to 30 ms required by the VSI-UPQC. This difference has practical implications in microgrids, where the cycling frequency of storage is high. The efficiency at full load reaches 97.1% compared to 95.6%, resulting in a power loss savings of 210 W. The passive components are reduced in volume by 28%, achieving an estimated power density of 2.4 kW/L versus 1.8 kW/L, which indicates better thermal management and more efficient spatial use for installation. From an application standpoint, these characteristics make the proposed topology suitable for grid-edge microgrids with distributed renewable generation and battery storage, industrial facilities with sensitive process loads and nonlinear equipment loads, electric-vehicle charging infrastructure where bidirectional power flow and harmonic injection occur simultaneously, and rural or island-mode systems with no stiff grid support where tighter local voltage regulation is required without the use of electrolytic capacitor banks that degrade over time.

Concerning limitations, the current evaluation is limited to simulation under predefined disturbance profiles from a seven-day NSRDB database. The extent to which these profiles represent the overall statistical variability of real-world solar variability and load-switching events is an open question that would have to be resolved through hardware/prototype validation. The matrix-converter switching strategy also comes with the commutation complexity that requires the accurate current direction detection; any misidentification during overlapping switching periods may cause current spikes that are not fully replicated by the present simulation environment. Additionally, the adaptive gain tuning mechanism has been optimised for the particular load composition used in this study, and its robustness under significantly different impedance ratios or during rapid load connection and disconnection sequences has not been characterised. This limitation limits the generalisability of the reported settling-time and regulation-error figures to cases that are substantially different from the tested operating envelope.

6. Conclusion

This study examined the operation of a capacitorless matrix-converter-based UPQC designed to achieve simultaneous power quality compensation in a three-phase, four-wire microgrid with a 50 kW photovoltaic source and a 30 kW bidirectional battery. The results show that the proposed configuration outperforms both the APF-only and conventional VSI-UPQC topologies for all the categories of disturbances tested. The source-current Total Harmonic Distortion (THD) was decreased from 18.4% to 2.1%, and the voltage sag recovery time was found to be 12 ms with a regulation error of 0.01 pu. Voltage Unbalance Factor (VUF) was reduced from 3.0 percent to 0.5 percent, the power factor was close to 0.995, and bidirectional power reversals were achieved in 18 milliseconds with Point-Of-Common-Coupling (PCC) deviations limited to ±0.015 pu. Furthermore, full load efficiency was 97.1% and power density was 2.4 kW/L, which proved the practical compactness provided by the elimination of the DC link capacitor bank. These results support the use of the proposed topology in renewable microgrids, industrial plants with sensitive loads, and electric vehicle charging stations where harmonic injection and power flow from the grid to the load and vice versa are simultaneous. Nonetheless, the investigation is limited to simulation with a seven-day National Solar Radiation Data Base (NSRDB) data set, and the sensitivity of the commutation logic and load-specific gain tuning raises questions about hardware robustness and controller generalisability. Validation of the prototype under a wider range of operating conditions and in multi-microgrid coordination conditions is needed to fill in the gaps of the unresolved issues in future studies.

Conflicts of Interest

The author(s) declare(s) that there is no conflict of interest regarding the publication of this paper.

References

[1] Waqas Ahamd, and Irfan Ullah, “Unified Power Quality Conditioner Based Power Quality Improvement in Micro-Grid,” *2025 IEEE Texas Power and Energy Conference (TPEC)*, College Station, TX, USA, pp. 1-6, 2025. [CrossRef] [Google Scholar] [Publisher Link]

[2] Devendra Kumar et al., “A Meshed Hybrid Microgrid Configuration with Unified Power Quality Conditioner,” *IEEE Journal of Emerging and Selected Topics in Power Electronics*, vol. 13, no. 2, pp. 2489-2499, 2025. [CrossRef] [Google Scholar] [Publisher Link]

[3] Zakaria Reguieg et al., "ANN-based PV-Integrated Power Conditioning System for MPPT Optimization and Power quality Enhancement in Hybrid Microgrids," *Energy Reports*, vol. 15, pp. 1-17, 2026. [CrossRef] [Google Scholar] [Publisher Link]

[4] Devesh Raj Mani, Sivasubramanian Muthu, and Kumarasamy Kasilingam, "Enhanced Power Quality and Efficient Photovoltaic Integration with a PV-based Unified Power Quality Conditioner using Optimized MPPT Technique," *Electrical Engineering*, vol. 107, pp. 2015-2036, 2025. [CrossRef] [Google Scholar] [Publisher Link]

[5] S. Lakshmi Kanthan Bharathi, A. Manjula, and P. Veeramanikandan, "Enhancing Power Quality through the Integration of Hybrid Renewable Energy Sources and Multi-level Inverters with Unified Power Quality Conditioner," *Electrical Engineering*, vol. 107, pp. 14407-14428, 2025. [CrossRef] [Google Scholar] [Publisher Link]

[6] Eyo Sunday Abia, Akhikpemelo Abraham, and Okon Ekpenyong, "Power Quality Improvement in a Distribution Network Using Unified Power Quality Conditioner (UPQC)," *Soft Computing Fusion with Applications*, vol. 2, no. 4, pp. 269-279, 2025. [Google Scholar] [Publisher Link]

[7] Shiv Shambhu Choudhary, and Tripurari Nath Gupta, "Voltage Compensation and Power Quality Enhancement Using an Optimized Series Transformer in Microgrid Operations," *Smart Grids and Sustainable Energy*, vol. 10, 2025. [CrossRef] [Google Scholar] [Publisher Link]

[8] Dinesh Kumar Nishad, Amar Nath Tiwari, and Saifullah Khalid, "Multi-Objective Optimization Simulation of Unified Power Quality Conditioner (UPQC)," *International Journal of Theoretical & Applied Computational Intelligence*, vol. 2025, pp. 71-81, 2025. [CrossRef] [Google Scholar] [Publisher Link]

[9] S.S Dheeban, N. B. Muthu Selvan, and Umashankar Subramaniam, "Artificial Neural Network based Solar Energy Integrated Unified Power Quality Conditioner," *Energy Sources, Part A: Recovery, Utilization, and Environmental Effects*, vol. 47, no. 1, pp. 7336-7360, 2025. [CrossRef] [Google Scholar] [Publisher Link]

[10] Deepi Singh et al., "Battery-Assisted Unified Power Quality Conditioner for Power Quality Improvement in Tidal-Driven Seaport Microgrids," *2025 IEEE Electric Ship Technologies Symposium (ESTS)*, Alexandria, VA, USA, pp. 436-443, 2025. [CrossRef] [Google Scholar] [Publisher Link]

[11] Bhanu Ganesh Lukka, Mercy Rosalina Kotapuri, and T.Rama Subba Reddy, "Intelligent Power Quality Improvement in Renewable Energy Microgrids using ANFIS-based UPQC," *2025 3rd International Conference on Sustainable Computing and Data Communication Systems (ICSCDS)*, Erode, India, pp. 1780-1785, 2025. [CrossRef] [Google Scholar] [Publisher Link]

[12] Ibrahim Abdulwahab et al., "Optimized Unified Power Quality Conditioner for Nonlinear Load Connected Microgrid Using Artificial Rabbit Search Optimization," *2025 IEEE Industrial Electronics and Applications Conference (IEACon)*, Kota Kinabalu Sabah, Malaysia, pp. 143-147, 2025. [CrossRef] [Google Scholar] [Publisher Link]

[13] Juan S. Espinosa Gutiérrez, and Alexander Aguila Téllez, "Optimal Placement of a Unified Power Quality Conditioner (UPQC) in Distribution Systems Using Exhaustive Search to Improve Voltage Profiles and Harmonic Distortion," *Energies*, vol. 18, no. 17, pp. 1-48, 2025. [CrossRef] [Google Scholar] [Publisher Link]

[14] K. Kanchana et al., "Advancing Microgrid Power Quality: Integration of GRU-based Control in PV-UPQC Systems," *Electrical Engineering*, vol. 107, pp. 223-248, 2025. [CrossRef] [Google Scholar] [Publisher Link]

[15] Muhammad Saleh Waseem Abbasi et al., "Power Quality Optimization Framework for Three Phase Microgrids with Grid Tied Solar PV and Battery Storage under Nonlinear Loads," *Scientific Reports*, vol. 15, pp. 1-45, 2025. [CrossRef] [Google Scholar] [Publisher Link]

[16] P. Rajesh, Francis H. Shajin, and L. Umasankar, "A Novel Control Scheme for PV/WT/FC/Battery to Power Quality Enhancement in Micro Grid System: A Hybrid Technique," *Energy Sources, Part A: Recovery, Utilization, and Environmental Effects*, vol. 47, no. 1, pp. 9126-9142, 2025. [CrossRef] [Google Scholar] [Publisher Link]

[17] Annu Dagar, Pankaj Gupta, and Vandana Niranjan, "Power Quality Analysis of q-Axis Current Injection-Based Islanding Detection Techniques," *IEEE Access*, vol. 13, pp. 205428-205438, 2025. [CrossRef] [Google Scholar] [Publisher Link]

[18] Gunasekaran Subramaniam, and Nandakumar Sundararaju, "Maximising Power Quality in Solar Photovoltaic Systems through Unified Power Quality Conditioners Integration using Enhanced Strategy," *Australian Journal of Electrical and Electronics Engineering*, pp. 1-16, 2025. [CrossRef] [Google Scholar] [Publisher Link]

[19] Nagaraju Samala, and Chandramouli Bethi, "Harnessing Synergy: A Holistic Review of Hybrid Renewable Energy Systems and Unified Power Quality Conditioner Integration," *Journal of Electrical Systems and Information Technology* vol. 12, pp. 1-74, 2025. [CrossRef] [Google Scholar] [Publisher Link]

[20] Titus Oluwasuji Ajewole et al., "Operational Improvement of Hybrid-source Microgrid using Unified Power Quality Conditioner Optimized with Reinforcement Learning Brainstorm Algorithm," *Journal of Electrical Systems and Information Technology*, vol. 13, pp. 1-23, 2026. [CrossRef] [Google Scholar] [Publisher Link]